Sustainable Structure and Materials, *Vol. 3, No .1, (2020) 10-24*
DOI: https://doi.org/10.26392/SSM.2020.03.01.010

Iterative Approach for Global and Local Stability of Built-up Stiffened Box Sections

Osama Bedair, PhD., P.Eng

OB Engineering Ltd., 415-249 Craig Henry Drive, Ottawa, Ontario, Canada
Corresponding author/ E-mail address: obedair@gmail.com

(*Received November 29, 2019, Revised January 02, 2020, Accepted January 03, 2020)*

ABSTRACT. *This paper describes iterative procedure for stability analysis of stiffened built-up stiffened box sections subject to combined loadings. Unconstrained optimization algorithm (UOA) is used to compute the global and local buckling stresses. Energy formulation is first presented for the structural elements assuming the stiffeners are rigidly connected to the flanges. Global buckling load is determined by minimizing the unconstrained objective function with respect to the displacement coefficients. The webs are assumed as partially restrained against rotation and subject to non-uniform compressive and shear loadings. Web local buckling is formulated using (UOA) by treating the skew angle and half wave length as design variables. Results are presented to illustrate structural performance of the assembled box section. Design guidelines are proposed that can be utilized in practice to maximize the structural response.*

Keywords; Box sections, structural stability, stiffened plates, steel structures, hollow sections.

1. INTRODUCTION

Built-up box sections are widely used in many engineering applications. Examples are box girder bridges, equipment and platform supports, conveyors and offshore structures. Built up box section can be fabricated by assembling individual plate elements or by joining two cold-formed C-sections face to face. The former approach allows the designer to use different flange and web thicknesses in order to reduce overall weight. In the second approach, two channels are fastened using self-drilling screws. The combined channels act together to resist induced the applied loading. The application of cold formed steel built-up box sections has been very popular in low or mid-rise residential and commercial buildings in North America. It is common in practice to stiffen the flanges to increase structural performance.

Box sections components may buckle locally or globally during operation. Several analysis and experimental procedures were developed in the past to demonstrate the structural performance. Early efforts by Vlasov [1] contributed to the development of simplified one dimensional beam element model that is popular in the industry to simulate the response of box sections with single or multiple spans. Refined analytical and numerical models also emerged utilizing advanced numerical analysis procedures such as Finite Element or Finite strip methods to analyze box sections using two or three dimensional stresses and displacement. Table (1) summarizes recent investigations done for box sections. The first column provides the reference number in square bracket. The second column briefly describes the investigation scope.

Table-1: Summary of investigations for box sections

Reference [No]	Investigation Description
[2]	Behavior of built-up cold formed steel box sections subject to axial compression
[3]	Stability of box section subject to eccentric axial loading.
[4]	Flexural torsional buckling of box sections subjected to eccentric force.
[5]	Influence of stiffener rigidity on buckling loads of flanges.
[6]	Boundary Element formulations for analysis of stiffened flanges.
[7]	Presented simplified models for analysis of box beam sections
[8]	Local and global buckling of stainless steel columns.
[9]	Effect of internal bracings on local buckling of hollow sections.
[10]	Capacity of box section subject compression and bending.
[11]	Influence of flange ductility for short steel box columns.
[12]	Analysis of stiffened composite using Fourier series approximations
[13]	Experimental data of stainless steel members.
[14]	Finite Element modeling strategies for orthotropic box sections.
[15]	Analysis of composite box sections using used Mindlin shear deformation model.

Box sections are sometimes filled with concrete to increase compressive and flexural capacity. The interior concrete material in this case restrains the attached box section plate components against inward buckling. The increase in buckling strength of these composite sections may reach 40% in. Local buckling of box sections filled with concrete has also received the attention of several researchers. Chen, et.al., [16] presented experimental and numerical investigations to examine performance of axially compressed steel tubes. Song, et. al. [17] investigated local buckling of high strength box steel sections with concrete infill using Finite Element procedure. Other investigations were reported by Lam and Williams [18], Liang [19], Ge [20] and Sakai et al. [21].

Built up box structural elements are frequently subject to various load combinations including compression and biaxial bending moments and shear. Therefore, stability is a critical design criterion. Furthermore, local web shear buckling is critical for deep box sections. Limited guidelines in design codes and engineering standards [22- 32] are available in practice for analysis of box sections subject to load combinations including shear loading. Much of the investigations focused to develop numerical or empirical analysis procedures for box sections under compression or bending.

References [33-37] illustrated static and dynamic response of walled sections. In some loading conditions FE and FS procedures require excessive computer time and consequently may not be practical for analysis of box section assemblies. Objective of this paper is to provide alternative numerical iterative procedure that can be used to predict global and local buckling of built-up stiffened box sections. The mathematical formulations are first presented for the box section components. Unconstrained optimization algorithm (UOA) is then described to compute global and local buckling. Results are also presented to illustrate the behavior of box sections. Design guidelines are proposed to maximize the structural response. Comparison with FS and FE is also provided.

2. FLANGE FORMULATIONS

Consider stiffened box section assembly shown in Fig.(1) of length (L), subject to combined compressive force (P) and biaxial moments (M_1, M_2), in the directions shown. The web and flange sizes are denoted by (b_w,t_w) and (b_f,t_f), respectively. The top and bottom flanges are denoted by (TF, BF), and the webs are denoted by (LW, RW) as shown in Fig.(1). Longitudinal stiffeners are attached to the top flange (TF) that are characterized by cross sectional area= (A^{LS}), first moment of inertia=(Q^{LS}), major and minor second moments of inertia {I^{LS}_y,I^{LS}_z} and torsional rigidity = (J^{LS}). The number of longitudinal and stiffeners are

denoted by NLS. Note that the application of moments (M_1 , M_2) causes the applied stress to vary across the webs and the flanges.

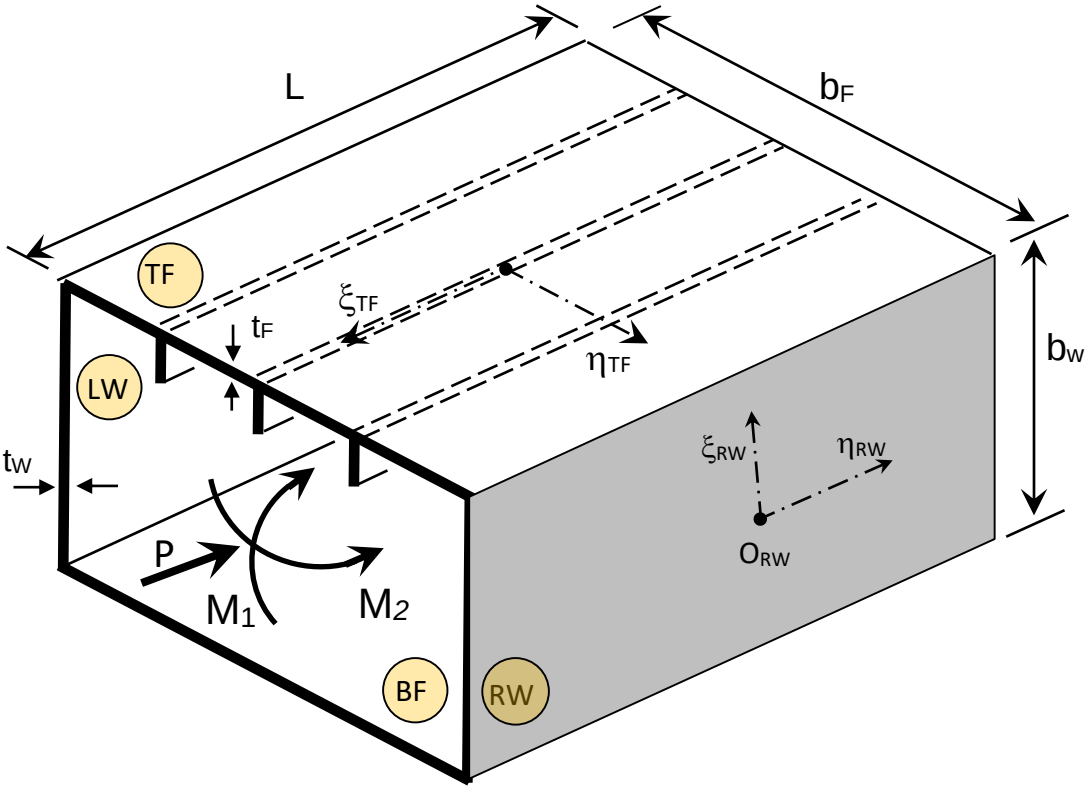

Fig-1: Typical Box section Assembly

In the present formulation, the following non-dimensional parameters are used to relate the web and the flange sectional properties;

$$\theta = \frac{b_w}{b_F}, \quad \varepsilon = \frac{t_w}{t_F} \tag{1}$$

The stiffened top flange (TF) out-of-plane and in-plane displacement functions (W^{TF}, U^{TF}, V^{TF}) are assumed as follow;

$$\begin{bmatrix} W^{TF}(\eta_{TF},\xi_{TF}) \\ U^{TF}(\eta_{TF},\xi_{TF}) \\ V^{TF}(\eta_{TF},\xi_{TF}) \end{bmatrix} = \begin{bmatrix} \sum_{i=1}^{M_1}\sum_{j=1}^{N_1} A_{ij}^{TF} & 0 & 0 \\ 0 & \sum_m\sum_n C_{mn}^{TF} & 0 \\ 0 & 0 & \sum_r\sum_z D_{rz}^{TF} \end{bmatrix} \begin{bmatrix} R_i^{TF}(\xi_{TF})\, Q_i^{TF}(\eta_{TF}) \\ P_m^{TF}(\xi_{TF})\, S_n^{TF}(\eta_{TF}) \\ T_r^{TF}(\xi_{TF})\, U_z^{TF}(\eta_{TF}) \end{bmatrix} \tag{2}$$

Where $\{R_i^{TF}(\xi_{TF}), Q_j^{TF}(\eta_{TF}), P_m^{TF}(\xi_{TF}), S_n^{TF}(\eta_{TF}), T_r^{TF}(\xi_{TF}), U_z^{TF}(\xi_{TF})\}$ are one dimensional shape functions that describes the top flange out of plane and in-plane displacement profiles, $\{A_{ij}^{TF}, C_{mn}^{TF}, D_{rz}^{TF}\}$ are the associated undetermined coefficients.

The top flange strain energy (SE^{TF}) is expressed in the following compact form;

$$SE^{TF} = \begin{bmatrix} TF^{1}_{mnpq} & TF^{2}_{mnrs} & TF^{3}_{mnijkl} & TF^{4}_{jkltfze} & TF^{5}_{rsgh} & TF^{6}_{rsijkl} & TF^{7}_{ijkl} \end{bmatrix} \begin{bmatrix} C_{mn}^{TF} C_{pq}^{TF} \\ C_{mn}^{TF} D_{rs}^{TF} \\ C_{mn}^{TF} A_{ij}^{TF} A_{kl}^{TF} \\ A_{ij}^{TF} A_{kl}^{TF} A_{tf}^{TF} A_{ze}^{TF} \\ D_{rs}^{TF} D_{gh}^{TF} \\ D_{rs}^{TF} A_{ij}^{TF} A_{kl}^{TF} \\ A_{ij}^{TF} A_{kl}^{TF} \end{bmatrix} \tag{3}$$

Where $\{TF^1 - TF^7\}$ are integral functions that contain the displacement profile and the sectional geometric properties. For example, TF^1, TF^2 and TF^3 have the following forms;

$$TF^{1}_{mnpq} = \frac{E\ t_F}{2(1-\nu^2)} \sum_{m=1}^{M1} \sum_{n=1}^{N1} \sum_{p=1}^{M3} \sum_{q=1}^{N3} \int_0^1 \int_0^1 \left[\frac{b_F}{L} \frac{\partial C_m}{\partial \xi_{TF}} \frac{\partial C_p}{\partial \xi_{TF}} D_n\ D_q + (1-\nu) \frac{L}{2b_f} C_m\ C_p \frac{\partial D_n}{\partial \eta_{TF}} \frac{\partial D_q}{\partial \eta_{TF}} \right] d\xi_{TF}\ d\eta_{TF} \tag{4}$$

$$TF^{2}_{mnrs} = \frac{E\ t_F}{2(1-\nu^2)} \sum_{m=1}^{M2} \sum_{n=1}^{N2} \sum_{r=1}^{M2} \sum_{s=1}^{N2} \int_0^1 \int_0^1 \left[2\nu \frac{\partial P_m(\xi)}{\partial \xi_{TF}} T_r\ S_n \frac{\partial U_s}{\partial \eta_{TF}} + (1-\nu)\ P_m \frac{\partial T_r}{\partial \xi_{TF}} \frac{\partial S_n}{\partial \eta_{TF}} U_s \right] d\xi_{TF}\ d\eta_{TF} \tag{5}$$

$$TF^{3}_{mnijk} = \frac{E\ t_F}{2(1-\nu^2)} \sum_{m=1}^{M2} \sum_{n=1}^{N2} \sum_{i=1}^{M1} \sum_{j=1}^{N1} \sum_{k=1}^{M2} \sum_{l=1}^{N2} \int_0^1 \int_0^1 \left[\frac{b_F}{L^2} \frac{\partial P_m}{\partial \xi_{TF}} \frac{\partial R_i}{\partial \xi_{TF}} \frac{\partial R_k}{\partial \xi_{TF}} S_n Q_j Q_l + \frac{\nu}{b_f} \frac{\partial P_m}{\partial \xi_{TF}} R_i R_k Q_n \frac{\partial Q_j}{\partial \eta_{TF}} \frac{\partial Q_l}{\partial \eta_{TF}} + \frac{1-\nu}{b_f} P_m \frac{\partial R_i}{\partial \xi_{TF}} R_k \frac{\partial S_n}{\partial \eta_{TF}} Q_j \frac{\partial Q_l}{\partial \eta_{TF}} \right] d\xi_{TF}\ d\eta_{TF} \tag{6}$$

By similar analogy, the bottom flange strain energy (SE^{BF}) can be formulated. The strain energy of typical longitudinal i^{th} stiffener (SE^{LSi}) attached to the top flange can be expressed as follow;

$$SE^{LSi} = \begin{bmatrix} LS^{1}_{ijkl} & LS^{2}_{ijmn} & LS^{3}_{ijmnkl} & LS^{4}_{ijkltfze} & LS^{5}_{ijkltf} & LS^{6}_{mnpq} & LS^{7}_{rsgh} \end{bmatrix} \begin{bmatrix} A_{ij}^{TF} A_{kl}^{TF} \\ C_{mn}^{TF} A_{ij}^{TF} \\ A_{ij}^{TF} C_{mn}^{TF} A_{kl}^{TF} \\ A_{ij}^{TF} A_{kl}^{TF} A_{tf}^{TF} A_{ze}^{TF} \\ A_{ij}^{TF} A_{kl}^{TF} A_{tf}^{TF} \\ C_{mn}^{TF} C_{pq}^{TF} \\ D_{rs}^{f} C_{gh}^{f} \end{bmatrix} \tag{7}$$

Where $[LS^1\text{-}LS^7]$ are integral functions that contain displacement and geometric parameters, given by;

$$LS^{1}_{ijkl} = \frac{E}{2} \sum_{i=1}^{M1} \sum_{j=1}^{N1} \sum_{k=1}^{M2} \sum_{l=1}^{N2} \int_0^1 \left[\frac{I_y^{LS}}{L^3} \frac{\partial^2 R_i}{\partial \xi_{LS}^2} \frac{\partial^2 R_k}{\partial \xi_{LS}^2} Q_j Q_l + \frac{1}{2(1+\nu)} \frac{J^{LS}}{b_F^3} \frac{\partial R_i}{\partial \xi_{LS}} \frac{\partial R_k}{\partial \xi_{LS}^2} \frac{\partial Q_j}{\partial \eta_{LS}} \frac{\partial Q_l}{\partial \eta_{LS}} \right] d\xi_{LS} \tag{8}$$

$$LS^{2}_{ijmn} = -\frac{EQ^{LS}}{L^{2}} \sum_{i=1}^{M1} \sum_{j=1}^{N1} \sum_{m=1}^{M2} \sum_{n=1}^{N2} \int_{0}^{1} \left[\frac{\partial P_m}{\partial \xi_{LS}} \frac{\partial^2 R_i}{\partial \xi_{LS}^2} S_n Q_j \right] d\xi_{LS} \quad (9)$$

$$LS^{3}_{ijmnkl} = \frac{EA^{LS}}{2L^{2}} \sum_{i=1}^{M1} \sum_{j=1}^{N1} \sum_{m=1}^{M2} \sum_{n=1}^{N2} \sum_{k=1}^{M2} \sum_{l=1}^{N2} \left[\int_{0}^{1} \frac{\partial P_m}{\partial \xi_{LS}} \frac{\partial R_i}{\partial \xi_{LS}} \frac{\partial R_k}{\partial \xi_{LS}} S_n Q_j Q_l \right] d\xi_{LS} \quad (10)$$

$$LS^{4}_{ijkltfze} = \frac{E A^{LS}}{8L^{3}} \sum_{i=1}^{M1} \sum_{j=1}^{N1} \sum_{k=1}^{M2} \sum_{l=1}^{N2} \sum_{f=1}^{M2} \sum_{z=1}^{N2} \sum_{t=1}^{M2} \sum_{e=1}^{N2} \int_{0}^{1} \left[\frac{\partial R_i}{\partial \xi_{LS}} \frac{\partial R_k}{\partial \xi_{LS}} \frac{\partial R_t}{\partial \xi_{LS}} \frac{\partial R_z}{\partial \xi_{LS}} Q_j Q_l Q_f Q_e \right] d\xi_{LS} \quad (11)$$

$$LS^{5}_{ijkltf} = \frac{EQ^{LS}}{2L^{3}} \sum_{i=1}^{M1} \sum_{j=1}^{N1} \sum_{k=1}^{M2} \sum_{l=1}^{N2} \sum_{t=1}^{M2} \sum_{f=1}^{N2} \int_{0}^{1} \left[\frac{\partial^2 R_i}{\partial \xi_{LS}^2} \frac{\partial R_k}{\partial \xi_{LS}} \frac{\partial R_t}{\partial \xi_{LS}} Q_j Q_l Q_f \right] d\xi_{LS} \quad (12)$$

$$LS^{6}_{mnpq} = \frac{E A^{LS}}{2L} \sum_{m=1}^{M2} \sum_{n=1}^{N2} \sum_{p=1}^{M2} \sum_{q=1}^{N2} \int_{0}^{1} \left[\frac{\partial P_m}{\partial \xi_{LS}} \frac{\partial P_p}{\partial \xi_{LS}} S_n S_q \right] d\xi_{LS} \quad (13)$$

$$LS^{7}_{rsgh} = \frac{E I_z^{LS}}{2L^{3}} \sum_{r=1}^{M2} \sum_{s=1}^{N2} \sum_{g=1}^{M2} \sum_{h=1}^{N2} \int_{0}^{1} \left[\frac{\partial^2 T_r}{\partial \xi_{LS}^2} \frac{\partial^2 T_g}{\partial \xi_{LS}^2} U_s U_h \right] d\xi_{LS} \quad (14)$$

The strain energy top flange transverse stiffener (SE^{TS}) can be formulated using similar analogy. The work done by the applied and restraining forces can also be expressed as follow;

$$WD^{TF} = \left[TF^{1}_{ijkl} \sum_{i=1}^{NLS} TF^{2}_{ijkl} \sum_{i=1}^{NLS} TF^{3}_{ijkl} \right] \begin{bmatrix} P^{TF} \\ SN^{LS} \\ SN^{TS} \end{bmatrix} A^{TF}_{ij} A^{TF}_{kl} \quad (15)$$

$$WD^{BF} = \left[BF^{1}_{ijkl} \right] [PBF] A^{BF}_{ij} A^{BF}_{kl} \quad (16)$$

Where

$$TF^{1}_{ijkl} = \sum_{i=1}^{M2} \sum_{j=1}^{N2} \sum_{k=1}^{M2} \sum_{l=1}^{N2} \int_{0}^{1} \int_{0}^{1} \left[\frac{b_F}{L} \frac{\partial R_i}{\partial \xi_{TF}} \frac{\partial R_k}{\partial \xi_{TF}} Q_j Q_j + \nu \frac{\varepsilon \theta}{1+\varepsilon \theta} \frac{L}{b_F} R_k R_i \frac{\partial Q_j}{\partial \eta_{TF}} \frac{\partial Q_j}{\partial \eta_{TF}} \right] d\xi_{BF} d\eta_{BF} \quad (17)$$

$$TFV^{2}_{ijkl} = \frac{A^{LS}}{2 t_F L} \sum_{i=1}^{M2} \sum_{j=1}^{N2} \sum_{k=1}^{M2} \sum_{l=1}^{N2} \int_{0}^{1} \left[\frac{\partial R_i}{\partial \xi_{TF}} \frac{\partial R_k}{\partial \xi_{TF}} Q_j Q_l \right] d\xi_{TF} \quad (18)$$

$$TFV^{3}_{ijkl} = \nu A^{TS} \frac{\varepsilon \theta}{t_F b_F (1+\varepsilon \theta)} \sum_{i=1}^{M2} \sum_{j=1}^{N2} \sum_{k=1}^{M2} \sum_{l=1}^{N2} \int_{0}^{1} \left[R_i R_k \frac{\partial Q_j}{\partial \eta_{TF}} \frac{\partial Q_l}{\partial \eta_{TF}} \right] d\eta_{TF} \quad (19)$$

$$BFV_{ijkl} = \sum_{i=1}^{M2} \sum_{j=1}^{N2} \sum_{k=1}^{M2} \sum_{l=1}^{N2} \int_{0}^{1} \int_{0}^{1} \left[\frac{b_F}{L} \frac{\partial R_i}{\partial \xi_{TF}} \frac{\partial R_k}{\partial \xi_{TF}} Q_j Q_l \right] d\xi_{BF} d\eta_{BF} \quad (20)$$

3. WEBS FORMULATIONS

For deep box sections, web local shear buckling is possible failure mode that may occur prior to the stiffened flanges. Due to the application of (M1) and (M_2), both webs are subject to different magnitude of compressive forces. For illustration, the compressive stress distribution at the left and right webs (RW) and (LW) are given by;

$$\sigma_{xx}^{RW} = \sigma_{xx} \left[\omega_I + 2\eta_{RW}\, \omega_{II} + 1 \right] \quad (21)$$

$$\sigma_{xx}^{LW} = \sigma_{xx} \left[\omega_I + 2\eta_{LW}\, \omega_{II} - 1 \right] \quad (22)$$

Where (σ^{RW}_{xx}, σ^{LW}_{xx}) are the applied stress variations across right and left webs (RW) and (LW) and (ω_I, ω_{II}) are non-dimensional stresses given by;

$$\omega_I = \frac{\sigma_1}{\sigma_{xx}} \quad , \quad \omega_{II} = = \frac{\sigma_2}{\sigma_{xx}} \quad (23)$$

Note that $\{\sigma_1, \sigma_2\}$ are bending stresses resulting from application of (M_1) and (M_2), respectively Therefore, each web is subject to non-uniform linearly varying compressive forces and shear forces. Noting that stress variation of Eqs.(21, 22) reveals that the right web (RW) is subject to a larger magnitude of compressive forces and hence may buckle prior to (LW).

By treating the webs as partially restrained against rotation the buckling load depends upon web/flange sizes. In the present formulation, the total shear forces acting on the longitudinal web edges are denoted by (τ). The inclusion of the shear forces causes the nodal lines in the buckling mode to be skewed. The oblique (or prime) coordinate system is related to the skew coordinates by using the phase angle (ϕ) as follow;

$$x_{RW} = x'_{RW} - y'_{RW} \tan\phi \ , \quad y_{RW} = y'_{RW} \sec\phi \quad (24)$$

The out-of-plane and in-plane displacement functions (W^{RW}, U^{RW}, V^{RW}) of the critical web (RW) are assumed as follow;

$$\begin{bmatrix} W^{RW}(\eta_{RW}, \xi_{RW}) \\ U^{RW}(\eta_{RW}, \xi_{RW}) \\ V^{RW}(\eta_{RW}, \xi_{RW}) \end{bmatrix} = \begin{bmatrix} \sum_{i=1}^{M_1} \sum_{j=1}^{N_1} A_{ij}^{RW} & 0 & 0 \\ 0 & \sum_m \sum_n C_{mn}^{RW} & 0 \\ 0 & 0 & \sum_r \sum_z D_{rz}^{RW} \end{bmatrix} \begin{bmatrix} R_i^{RW}(\xi_{RW})\ Q_i^{RW}(\eta_{RW}) \\ P_m^{RW}(\xi_{RW})\, S_n^{RW}(\eta_{RW}) \\ T_r^{RW}(\xi_{RW})\ U_z^{RW}(\eta_{RW}) \end{bmatrix} \quad (25)$$

Where $\{R_i^{RW}(\xi_{RW})$, $Q_j^{RW}(\eta_{RW})$, $P_m^{RW}(\xi_{RW})$, $S_n^{RW}(\eta_{RW})$, $T_r^{RW}(\xi_{RW})$, $U_z^{RW}(\xi_{RW})\}$ are the (RW) displacement functions and $\{A_{ij}^{RW}, C_{mn}^{RW}, D_{rz}^{RW}\}$ are the associated coefficients.

The strain energy (SE^{RW}) of the each web is composed of bending and rotational strain energy that can be expressed as;

$$SE^{RW} = \begin{bmatrix} BSE^{RW} & RSE^{RW} \end{bmatrix} \begin{bmatrix} 1 \\ 1 \end{bmatrix} \quad (26)$$

Where (BSE^{RW}) is the web bending strain energy, (RSE^{RW}) is rotational strain energy. Work done by shear and compressive forces can also be expressed as follow;

$$WD^{RW} = \begin{bmatrix} WDA^{RW} & WDR^{RW} \end{bmatrix} \begin{bmatrix} -1 \\ -1 \end{bmatrix} \quad (27)$$

Where (WDA^{RW}) is the work done by applied forces and (WDR^{RW}) is the work done by the restraining reactions.

4. UNCONSTRAINED OPTIMIZATION FORMULATION

Global stability of the box assembly can be computed by combining strain energies components given by equations (3,7,15,16,26,27). The total strain energy is expressed as follow

$$TSE = \begin{bmatrix} SE^{TF} & -WD^{TF} & \sum_{i=1}^{NLS} SE^{LSi} & \sum_{i=1}^{NTS} SE^{TSi} & SE^{BT} & -WD^{BF} & SE^{RW} & -WD^{RW} & SE^{LW} & -WD^{LW} \end{bmatrix} \begin{bmatrix} C_1 \\ C2 \\ C_3 \\ C_4 \\ C_5 \\ C_6 \\ C_7 \\ C_8 \\ C_9 \\ C_{10} \end{bmatrix} \quad (28)$$

Where (TSE) is the total strain energy of the assembled box section. C_1-C_{10} are control parameters that equal either (0) or (1), depending upon the buckling coefficient being determined. Values of (C) parameters are summarized in Table (2). For example, for global buckling of stiffened box section C_1-C_{10} = 1.

Table-2: Numeric values of C_1-C_{10} of Equation (29)

Buckling Coefficient	C_1	C_2	C_3	C_4	C_5	C_6	C_7	C_8	C_9	C_{10}
$\mathbf{K^{Global}}$	1	1	1	1	1	1	1	1	1	1
$\mathbf{K^{TF}}$	1	1	1	1	0	0	0	0	0	0
$\mathbf{K^{BF}}$	0	0	0	0	1	1	0	0	0	0
$\mathbf{K^{RW}}$	0	0	0	0	0	0	1	1	0	0
$\mathbf{K^{LW}}$	0	0	0	0	0	0	0	0	1	1

For unstiffened box section C_3=C_4=0. Similarly, the top flange local buckling stress can be obtained by setting C_1=C_2=C_3=C_4=1 and C_5-C_{10}=0, to obtain;

$$\sigma_{cr}^{TF} = K^{TF}\left(A_{ij}^{TF}, C_{mn}^{TF}, D_{rs}^{TF}\right)\frac{\pi^2 E}{12(1-\nu^2)}\left(\frac{t_F}{b_F}\right)^2 \quad (29)$$

Minimizing the buckling load factor (K^{TF}) with respect to displacement coefficients (A_{ij}^{TF}, C_{mn}^{TF}, D_{rs}^{TF}) leads to the following unconstrained optimization problem;

$$Minimize\ K\left(A_{ij}^{TF}, C_{mn}^{TF}, D_{rs}^{TF}\right) \quad (30)$$

$$Subject\ to \quad \begin{bmatrix} A_{ij}^{TF} \\ C_{mn}^{TF} \\ D_{rs}^{TF} \end{bmatrix}^{Lower} \leq \begin{bmatrix} A_{ij}^{TF} \\ C_{mn}^{TF} \\ D_{rs}^{TF} \end{bmatrix} \leq \begin{bmatrix} A_{ij}^{TF} \\ C_{mn}^{TF} \\ D_{rs}^{TF} \end{bmatrix}^{Upper} \quad (31)$$

The solution of the above unconstrained optimization algorithm (UOA) provides local buckling stress of the flange.

By similar analogy local buckling stress of the right web (RW) can be obtained by assembling strain energy components and using $C_7=C_8=1$ as follow;

$$(\sigma_1^{RW},\tau^{RW})_{cr} = K_{(P,S)}^{RW} \quad \frac{\pi^2 E}{12(1-\nu^2)}\left(\frac{t_w}{b_w}\right)^2 \tag{32}$$

Where E is modulus of elasticity and ν is Poisson's ratio and K^{RW} is buckling coefficient given by;

$$K_{(1,y,S)}^{RW} = \frac{RWJ_1 \sec^2(\phi) + 2\bar{\beta}_w^2\left[(1-\nu)+2\tan^2(\phi)\right]RWJ_2 + 2\bar{\beta}_w^2\left[\nu+\tan^2(\phi)\right]RWJ_3 - 4\bar{\beta}_w \tan(\phi)\sec(\phi)\,RWJ_4 + \frac{C\bar{\beta}_w^2}{Db}\sec(\phi)\left[RWJ_5 + RWJ_6\right]}{\pi^2\bar{\beta}_w^2\cos^2(\phi)\left[F_1 RWL_W(\xi,\bar{\eta}) + +2F_{xy}\bar{\beta}_w\left(RWJ_9 - \frac{1}{\bar{\beta}_w}\sin(\phi)\,RWJ_{10}\right)\right]} \tag{33}$$

Where RWJ_1- RWJ_{10} are integral functions that contain displacement profiles and geometric properties. The unconstrained optimization problem in this case is expressed as;

$$Minimize\ K\left(A_{ij}^{TF}, C_{mn}^{TF}, D_{rs}^{TF}, \phi, \frac{\bar{\lambda}}{\bar{b}}\right) \tag{34}$$

$$Subject\ to \begin{bmatrix} A_{ij}^{TF} \\ C_{mn}^{TF} \\ D_{rs}^{TF} \\ \phi \\ \lambda \end{bmatrix}^{Lower} \leq \begin{bmatrix} A_{ij}^{TF} \\ C_{mn}^{TF} \\ D_{rs}^{TF} \\ \phi \\ \lambda \end{bmatrix} \leq \begin{bmatrix} A_{ij}^{TF} \\ C_{mn}^{TF} \\ D_{rs}^{TF} \\ \phi \\ \lambda \end{bmatrix}^{Upper} \tag{35}$$

Note that due to the presence of the shear, the phase angle and half wave length (ϕ,λ) are treated as design variables. The above unconstrained optimization problem can be solved using Sequential Quadratic Programming. The objective is to find for prescribed functions displacement functions and geometric parameters, the design variables that minimize the K factor given by Eqs. (30) or (34).

The minimization strategy of Sequential Quadratic Programming is determined through an iterative procedure described by;

$$x_i^{k+1} = x_i^k + \beta^k\ \zeta^k \qquad k = 0,1,2,3,... \tag{36}$$

Where the superscript (k) represents the iteration number and subscript (i) denotes the number of design variables, (x) is a vector containing these variables, (β) is a step size and (ζ) is a search direction vector that is determined by generating and solving a sequence of quadratic sub-problems. In each iteration, the search direction and step length are computed to reduce the objective function. At typical k^{th} iteration, the search direction is computed from the solution of the quadratic, Taylor expansion of the buckling coefficient (K);

$$minimize\ \nabla K\left(A_{ij}^{TF}, C_{mn}^{TF}, D_{rs}^{TF}, \phi, \frac{\bar{\lambda}}{\bar{b}}\right)\zeta + \frac{1}{2}\zeta^T \nabla^2 K\left(A_{ij}^{TF}, C_{mn}^{TF}, D_{rs}^{TF}, \phi, \frac{\bar{\lambda}}{\bar{b}}\right)\zeta \tag{36}$$

Where $\nabla K = \partial K/\partial x_i$ is the gradient of the buckling coefficient at the k^{th} iteration and $\nabla^2 K$ is the Hessian matrix given by;

$$\nabla^2 K = \begin{bmatrix} \frac{\partial^2 K}{\partial x_1^2} & \frac{\partial^2 K}{\partial x_1 \partial x_2} & \cdots & \frac{\partial^2 K}{\partial x_1 \partial x_j} \\ \vdots & \vdots & \cdots & \vdots \\ \frac{\partial^2 K}{\partial x_i \partial x_1} & \frac{\partial^2 K}{\partial x_i \partial x_2} & \cdots & \frac{\partial^2 K}{\partial x_i \partial x_j} \end{bmatrix} \quad (37)$$

After obtaining the search direction, each iteration proceeds by determining a step length (ζ) that produces sufficient decrease in the objective function. The process continues until the decrease in (K) is negligible.

5. Numerical Verification and Results

Accuracy of the (UOA) is compared in Table (3) with the numerical values presented by Pham and Hancock [38] using semi-analytical finite strip (FS) method. The comparison is made for (θ) = 1.67, 2, 2.5, 3.33, 5 and 10. In the (FS) solution, the web was discritized using 16 longitudinal strips and the flanges using 10 strips. The values of the unconstrained optimization algorithm (UOA) were obtained by minimizing the non-linear expression of (K^{RW}) given by Eq.(33). As can be seen in Table (3) the prediction of both methods is within reasonable agreements. The average difference between (UOA) and the Finite Strip analysis is approximately 7%.

Table-3: Comparison of Shear Buckling K^{RW} factor for partially restrained condition

θ	**FS Ref. [38]**	**Present [UOA]**
1.67	6.81	7.40
2	6.72	7.18
2.5	6.60	6.81
3.33	6.43	6.60
5	6.19	6.30
10	5.88	6.00

Fig.(2) shows the top flange local buckling load factor (K^{TF}) obtained using (UOA) with the flange/web thickness ratio (ε) for built-up stiffened box section. Modulus of Elasticity E=200 GPa and Poisson's ratio ν=0.33. The curve with solid circles represents a flange with six equally spaced stiffeners (NLS=6). The curve with solid triangles represents a flange with five stiffeners (NLS=5). It can be noted that the variations in the buckling load factor is influenced by the flange and the web geometric proportions.

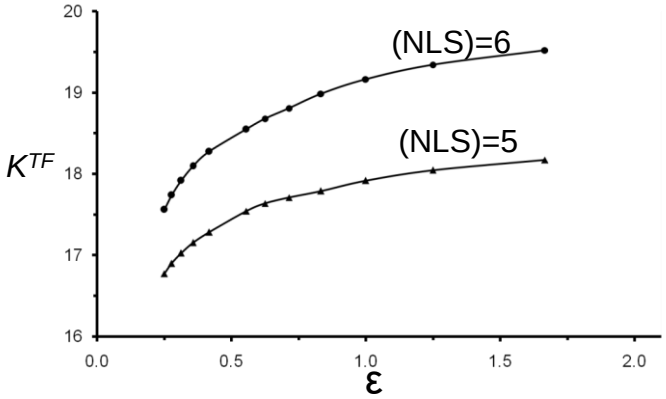

Fig.-2: Buckling Coefficient (K) vs. (t_f/t_w) for NLS=5, 6.

In both cases, a rapid increase in the (K^{TF}) factor is observed in the early stages. The increase is more pronounced as the number of stiffeners increases. As illustration, For (ε)= 0.63, the (K^{TF}) = 17.7 for (NLS=5). This value increases to (K^{F}) =18.6 by adding a stiffener (NLS=6). It worthwhile noting that the increase in (K^{TF}) for NLS=5 ranges between (16.8 and 18.3) by increasing (ε) from 0.25 to 2.25. This range is widened for (NLS=6) to 17.4 and 19.8. To illustrate cost efficiency, assume it is required to design a flange section for buckling stress of σ^{TF}_{cr} = 250 MPa. Therefore, by using six stiffeners, the overall weight of the box girder to prevent this local buckling stress is 6.3 tons. If this (σ^{TF}_{cr}) to be achieved without using stiffeners, the weight of the box girder should increase to 9.3 tons by adjusting the flange thickness. This corresponds to almost 55% increase in weight.

Fig.3 shows stability design space of box section subject to uniform compression. The buckling coefficient (K) variation with (ε) is shown for (θ) = 1.5. The curve with circle legends represents the flange domination while the triangles represent the range of (ε) when the web dominates buckling. The point of intersection (K)=6.65 at (ε)= 0.88 represents the optimum design when both flange and web buckle simultaneously. Therefore, the flange dominates buckling load for in the range (ε) ≥ 0.86. If the engineer, for example decides to use a flange width of 900 mm, web width 800 mm, and web thickness of 14 mm. The optimum flange thickness required in this case is 12mm. Therefore, the feasible stability domain is the area below the curves.

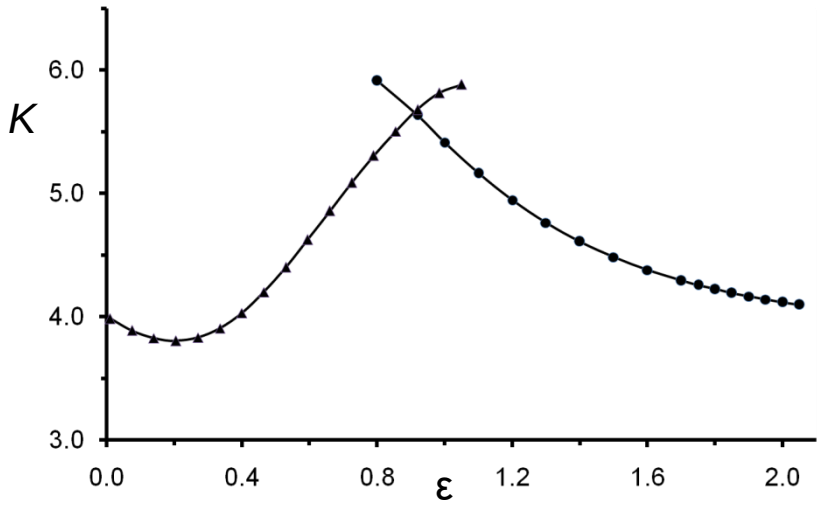

Fig.-3: Box section Stability Boundary

Fig. (4) shows the influence of the web on buckling stress of the top flange. For convenience, the top flange end stresses are related by the parameter (ρ) defined as;

$$\rho = \left(\frac{\sigma_{XX} + \sigma_2 - 1}{\sigma_{XX} + \sigma_2 + 1} \right) \tag{38}$$

The buckling stress of top flange (σ^{TF}_{buc}) is plotted vs. parameter (θ) for bending ratio ($\mu=M_2/M_1$) =0.25. The box section parameters are; (E)=200 GPa, (ν)=0.33, (L)= 3000 mm and (ε)=1. Curves with solid circles represents stress gradient (ρ)= 0.1 and triangular legend represents (ρ)=0.6. The parameter (θ) varies between 0.25 and 3. As shown, by increasing (θ) the buckling stress (σ^{TF}_{buc}) increases due to the increase of the rotational restraints. The values of (σ^{TF}_{buc}) increase by almost 100% by increasing the web/flange width ratio (θ) from 0.2 to 2.8. It should be noted that much of the increase in (σ^{FT1}_{buc}) occurs between (θ)=0.2 and 1.8. Beyond this range the influence of (θ) on flange buckling stress is very little. It must be noted that code prediction for (μ)=0 is constant value (σ^{TF}_{buc})=141 MPa. The difference is 40% by accounting for web rotational restraints.

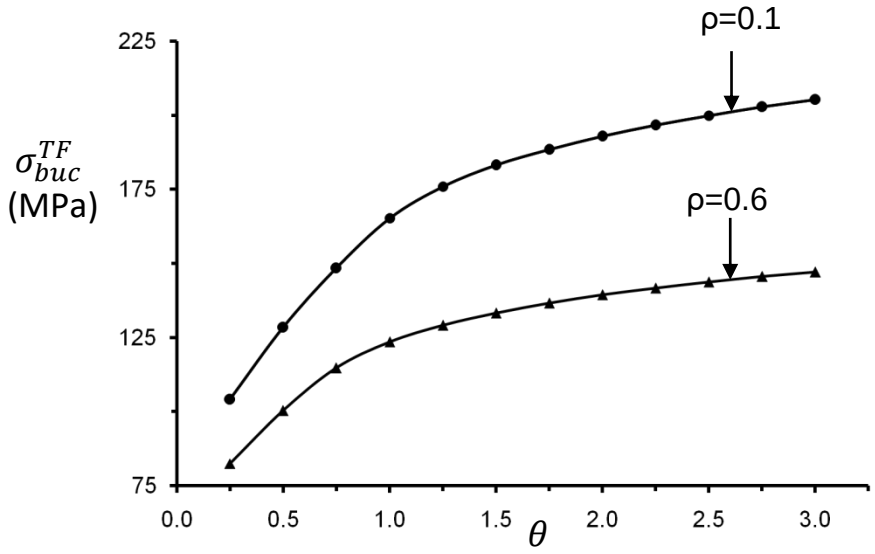

FIG-4: Variation of ($\sigma^{F1}{}_{buc}$) with (θ) for ρ=0.1, 0.6

The variation of moment ratio parameter ($\mu=M_2/M_1$) with top flange buckling coefficient (K^{TF}) is depicted in Fig (5). In this case, E=200 GPa ν=0.33., (ε)=1, L=2700 mm and (σ_{xx}/σ_1) = 1. The curve circular legends represents (θ)=1 and the triangular legend represents (θ) =10. Both curves intersect with the vertical y-axis at (μ) = 0. This point represents the uniaxial compression and bending loading condition. In both cases, buckling load coefficient (K^{TF}) decreases by increasing the stress ratio (μ) until each curve reaches a constant value. It can also be observed that as the web size increases, the (K^{TF}) factor increases due to the increase the flange rotational restraint. The increase is very pronounced for small (θ) variations. To illustrate, the average increase of (K^{TF}) is almost 30% by increasing (θ) from 1 to 10. This shows sensitivity of the top flange buckling load factor with (θ). It should be emphasized that current design codes [22-32] provide a constant value of for all values of (θ). It was noted that in some cases the difference may exceed 38%.

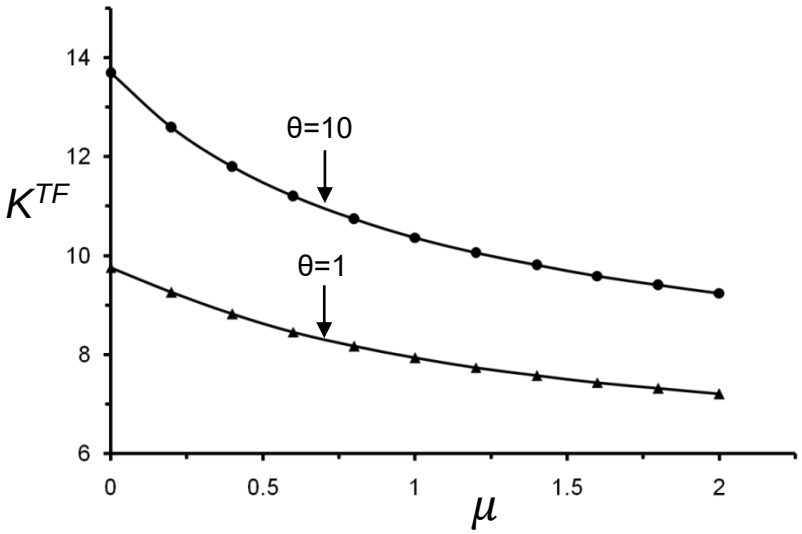

FIG.-5: Variation of (K) with (μ) for (θ)=1, 10

It is of interest to show in influence of flange thickness on shear buckling of the web (K^{RW}). Fig.(6) shows the variation (K^{TF}) with (θ). The triangular data points represents (θ) = 1.2 and the solid circles (θ)= 1.75. The variation of (θ) ranges between 0.2 and 3. The change in (K^{RW}) values is approximately 14% for (ε) =1.75. This difference increases to 24% by decreasing (ε) to 1.2. Therefore, as the flange width increases the shear buckling load factor (K^{RW}) increases due to the increase in the flange rotational stiffness. It can be observed that majority of the increase in the (K^{RW}) values occur in the early stages of the both curves. The change becomes very small when the (θ) ratio approaches 1. Accordingly, additional material is not economical beyond this value.

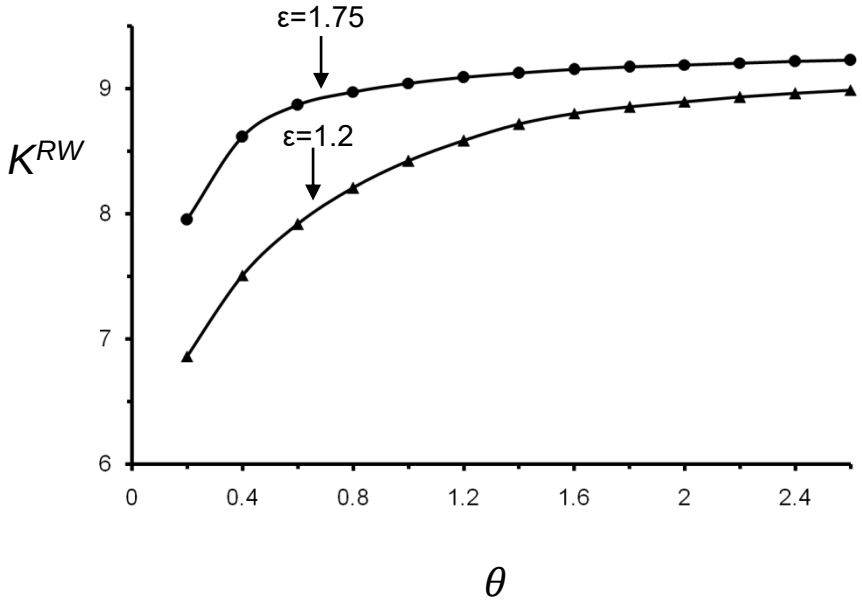

FIG-6: Web shear buckling coefficient (K^{RW}) with (θ).

6- CONCLUSIONS

Limited literature dealt with local stability of stiffened box sections subject to combined loadings. This loading arrangement is encountered in several engineering applications. Much of the effort was directed towards investigating box sections members subjected either to uniform compression or pure bending. The paper described efficient iterative algorithm using unconstrained optimization algorithm (UOA) to compute global and local buckling of built-up stiffened box section subject to combined loadings. Energy formulation for the top stiffened flange and the attached webs was presented. The stiffeners are assumed to be rigidly connected to the top flange. Unconstrained optimization algorithm was then described to compute the global and local buckling of assembled box components. Results were presented to illustrate behavior of box section. Design guidelines are proposed that be utilized in practice to maximize the structural response.

7- REFERENCES

1] Vlasov V. Thin-walled elastic beams. Washington, DC: National Science Foundation, 1961.

2] Roy K., Ting T C, Lau H, Lim J. Experimental and numerical investigations on the axial capacity of cold-formed steel built-up box sections. Journal of Construction Steel Research, 2019, 160 :411-427

3] L P., Yang Y., Yuan J., Jia B. Numerical investigation into prestressed stayed steel box section columns under eccentric loading, Journal of Construction Steel Research, 2019, 159:1-12.

4] Hsu H, Tsao J. Flexural–torsional performance of thin-walled steel hollow box columns subjected to a cyclic eccentric load. Thin-Walled Structures, 2007, 45 (2):149–58.

5] Choi B. , Yoo C. "Strength of stiffened flanges in horizontally curved box girders" Journal of Engineering Mechanics, 2005, 131 (2): 167-176.

6] Wen P.; Aliabadi M., Young A.; ”Boundary element analysis of shear deformable stiffened plates”. Engineering Analysis with Boundary Elements, 2002, 26 :511-520.

7] Jeon S., Cho M., Lee I. Static and dynamic analysis of composite box beams using large deflection theory. Computers and Structures; 1995, 57(4):635–642.

8] Gonçalves R, Camotim D. local and global buckling analysis of aluminium and stainless steel columns. Computer and Structure, 2004, 82(17):1473–1484.

9] Hsu H, Juang L, "Performance of thin-walled box columns strengthened with internal braces, Thin-Walled Structures, 2000, 37: 241–258

10] Cetinkaya O., Nakamura S., Takahashi K. Ultimate strain of stiffened steel box sections under bending moment and axial force fluctuations, Engineering Structures, 2009, 31: 778–787

11] Zheng Y, Usami T, Ge H. Ductility of thin-walled steel box stub-columns. J Struct Eng ASCE, 2000, 126 (11):1304–1311.

12] Nath S, Ahmed S, Kim S. Analytical solution of a stiffened orthotropic plate using alternative displacement potential approach. Proceedings of the Institution of Mechanical Engineers, Part G: Journal of Aerospace Engineering, 2010, 224 (1): 89-99.

13] Young B, Hartono W. Compression tests of stainless steel tubular members. J Struct Eng, ASCE, 2002; 128(6):754–761

14] Jiang W. Bao G., Robert J. “Finite element modeling of stiffened and unstiffened orthotropic plates” Computers & Structures, 1997, 63:105-117

15] Zhang H, DesRoches R, Yang Z., Liu S. Experimental and analytical studies on a streamlined steel box girder, Journal of Constructional Steel Research, 2010, 66:906–914

16] Chen J, Li W., Han L., Wang F., Mu, T. Structural behaviour of concrete-encased CFST box stub columns under axial compression, Journal of Construction Steel Research, 2019, 158:248-262.

17] Song Y., Li J., Chen Y. Local and post-local buckling of normal/high strength steel sections with concrete infill, Thin Walled Structures , 2019, 138: 55-169

18] Lam D, Williams C. Experimental study on concrete filled square hollow sections. Steel and Composite Structures, 2004, 4(2):95–112.

19] Liang Q. Strength and ductility of high strength concrete-filled steel tubular beam-columns. Journal of Constructional Steel Research, 2009, 65(3):687–98.

20] Ge H, Gao Sh, Usami T. Stiffened steel box columns. Part 1: Cyclic behaviour. Earthq Eng Struct Dyn; 2000, 29:1691–706.

21] Sakai T, Sakino K, Ishibashi H. Experimental studies on concrete-filled square steel tubular short columns subjected to cyclic shearing force and constant axial force. Trans Architectural Institute of Japan (Tokyo),1985, 353: 81–91.

22] AISI. North American Specification for the Design of Cold-Formed Steel Structural Members. American Iron Steel Institute, Washington DC, USA, 2007

23] AISC. Steel Construction Manual. 4th Edition. American Institute of Steel Construction, Chicago, USA, 2006.

24] ASCE/SEI 7-10 7. Minimum Design Loads and other structures. American Society of Civil Engineers, Virginia, USA, 2010.

25] AASHTO LRFD Bridge Design Specifications, American Association of State Highway and Transportation “-Customary US units “ AASTO Publications, Washington, USA, 2012.

26] CRC. Handbook of Structural Stability. Column Research Committee of Japan, Corona Publishing Co., Tokyo, Japan, 1971.

27] CSA-S136-07. North American Specification for the Design of Cold-Formed Steel Structural Members”, Canadian Standard Steel Association, Mississauga, Ontario, Canada, 2007.

28] CAN/CSA-S16-01.Limit states design of steel structures. Canadian Standards Association, Mississauga, Ontario, Canada, 2007.

29] Eurocode 3. Design of steel structures Part 1.5: plated structural elements; EN 1993-1-5: 2005.

30] Gaylord E., Gaylord C., editors. Structural engineering handbook. McGraw-Hill, USA, 1996.

31] Ziemian R., editor. Guide to Stability Design Criteria for Metal Structures. 6th edition, John Wiley and Sons Ltd. 2010

32] Beedle L., editor. Stability of metal structures, a world view. 2nd Ed., Structural Stability Research Council, USA, 1991.

33] Bedair O. Guidelines for Design of Transversely Stiffened Thin Walled Steel Plates. Recent Patents on Engineering, 2016, 10 (1):69-76.

34] Bedair O. Novel Design Procedures For Rectangular Hollow Steel Sections (RHSS) Subject To Compression, Major & Minor Axes Bending. ASCE, Practice Periodical on Structural Design and Construction, 2015, Vol. 20, 04014051

35] Bedair O. Modern Steel Design and Construction Used In Canada's Oil Sands Industry. Journal of Steel Design Construction and Research, 2014, 7 (1): 32-40

36] Bedair O. Rational Design of Pip-Racks Used For Oil Sands and Petrochemical Facilities. ASCE, Periodical on Structural Design and Construction, 2014, (4), 04014029.

37] Bedair O. "Analysis and Limit State Design of Stiffened Plates and Shells: A World View. Journal of Applied Mechanics Reviews, 2009, Vol. 62 :1-16.

38] Pham C., Hancock G. Shear buckling of thin-walled channel sections. Journal of Constructional Steel Research, 2009, 65: 578-585

- NOTATIONS

A_{ij}^{TF}, C_{mn}^{TF}, D_{rz}^{TF} = top flange displacement coefficients;
A^{LS}, Q^{LS}, I^{LS}_{y}, I^{LS}_{z} , J^{LS} = longitudinal stiffener area, first moment of inertia, major/ minor second moment of inertia and torsional rigidity
AWD^{RW} = work done by applied forces
A_{ij}^{RW}, C_{mn}^{RW}, D_{rz}^{RW} = web displacement coefficients.
b_w = web width;
b_F= flange width;
BSE^{RW}= web bending strain energy,
C_1-C_{10} = control parameters
E = elastic modus
K^{RW} , K^{LW} , K^{TF} , K^{BF}= web and flange buckling coefficients;
L = length of the box section;
LS^1- LS^7 = stiffeners integral functions
LS = longitudinal stiffeners;
M_1, M_2= Major and minor axes bending moments.
NLS = Number of longitudinal and stiffeners;
O_{RW}, o_{TF} = Web and flange origins
P = Applied axial force;
R_i^{TF}, Q_j^{TF}, P_m^{TF}, S_n^{TF}, T_r^{TF}, U_z^{TF} = one dimensional shape functions
R_i^{RW}, Q_j^{RW}, P_m^{RW}, S_n^{RW}, T_r^{RW}, U_z^{RW} = web displacement functions
RSE^{RW} = rotational strain energy,
RWD^{RW} = work done by the restraining reactions.
RWJ_i- RWJ_{10} = integral functions
SE^{TF} = The top flange strain energy;
SE^{TS} = transverse stiffener strain energy
SE^{RW}= web strain energy
TF^1 -TF^7 = integral functions
t_w, t_F = web and flange thickness;
W^{RW}, U^{RW}, V^{RW} = out-of-plane and in-plane displacement functions
x= design variables
ξ_{RW}, η_{RW} , ξ_{RW}, η_{RW}, ξ_{TF}, η_{TF}, ξ_{TF}, η_{TF} = webs and flanges local coordinates;
ϕ = phase angle
λ = half the wave length
β= step size
ζ= search direction vector
ε = non-dimensional parameter (t_F/t_w)
θ= non-dimensional parameter (b_w/b_F)
μ= non-dimensional parameter M_2/M_1
τ= Web shear stress.
σ^{RW}_{buc}, σ^{TF}_{buc} = web and flange critical buckling stresses;
σ^{TF}_{xx}, σ^{BF}_{xx} = applied stress across the flanges
ω_I, ω_{II}= non dimensional stresses
v = Poisson ratio;